Available online at www.sciencedirect.com
ScienceDirect
Earth and Planetary Science Letters 260 (2007) 37–55
EPSL
www.elsevier.com/locate/epsl

Mantle peridotite xenoliths in andesite lava at El Peñon, central Mexican Volcanic Belt: Isotopic and trace element evidence for melting and metasomatism in the mantle wedge beneath an active arc

Samuel B. Mukasa [a,*], Dawnika L. Blatter [b], Alexandre V. Andronikov [a]

[a] *Department of Geological Sciences, University of Michigan, Ann Arbor, MI 48109-1005, USA*
[b] *Department of Earth and Planetary Science, University of California, Berkeley, CA 94720, USA*

Received 6 July 2006; received in revised form 3 May 2007; accepted 7 May 2007
Available online 13 May 2007
Editor: R.W. Carlson

Abstract

Peridotites in the mantle wedge and components added to them from the subducting slab are thought to be the source of most arc magmas. However, direct sampling of these materials, which provides a glimpse into the upper mantle beneath an active margin, is exceedingly rare. In the few arc localities where found, peridotite xenoliths are usually brought to the surface by basaltic magmas. Remarkably, the hornblende-bearing ultramafic xenoliths and clinopyroxene megaxenocrysts from El Peñon in the central Mexican Volcanic Belt were brought to the surface by a Quaternary high-Mg siliceous andesite, a rock type usually considered too evolved to be a direct product of mantle melting. The xenoliths and megaxenocrysts from El Peñon represent lithospheric mantle affected by significant subduction of oceanic lithosphere since as early as the Permian. Trace element and radiogenic isotope data we report here on these materials suggest a history of depletion by melt extraction, metasomatism involving a fluid phase, and finally, limited reaction between the ultramafic materials and the host andesite, probably during transport. They also show that high-Mg siliceous andesite can be a direct product of 1–5% melting of H_2O-bearing spinel lherzolite.

Keywords: peridotite xenoliths; arc settings; andesite; metasomatism; trace elements; radiogenic isotopes

1. Introduction

Direct measurement of the composition of the mantle wedge beneath volcanic arcs is vitally important to understand melt generation and the recycling of lithophile and volatile elements at subduction zones. Current characterization of the subduction-modified mantle wedge relies heavily on arc volcanic rocks, some of which have been contaminated by their interaction with the crust. A limited number of pioneering studies (Takahashi, 1980; Canil and Scarfe, 1989; Vidal et al., 1989; McInnes and Cameron, 1994; Kepezhinskas et al., 1995; Kepezhinskas et al., 1996; Brandon and Draper, 1996; McInnes et al., 2001) have recognized the importance of characterizing peridotite xenoliths thought to represent the mantle wedge beneath active subduction-related volcanic arcs. Most of these, however, have focused on peridotite xenoliths brought to the surface in back-arc settings by basaltic magmas. It is only in a few exceptional cases (Tanaka and Aoki, 1981; Conrad and Kay, 1984; Maury et al., 1992;

* Corresponding author. Tel.: +1 734 936 3227; fax: +1 734 763 4690.
E-mail address: mukasa@umich.edu (S.B. Mukasa).

0012-821X/$ - see front matter © 2007 Elsevier B.V. All rights reserved.
doi:10.1016/j.epsl.2007.05.013

Blatter and Carmichael, 1998; Parkinson and Arculus, 1999) that peridotite xenoliths were transported to the surface in andesitic scoriae and lava. Peridotite xenoliths in arc settings might provide a direct record of the composition of the lithospheric mantle wedge beneath active convergent margins, and illustrate the effects of metasomatism and partial melting associated with subduction in these regions.

El Peñon is the only known locality of peridotite xenoliths in the Mexican Volcanic Belt (MVB), and thus offers a uniquely important perspective on the record of subduction-zone processes in the mantle wedge. The

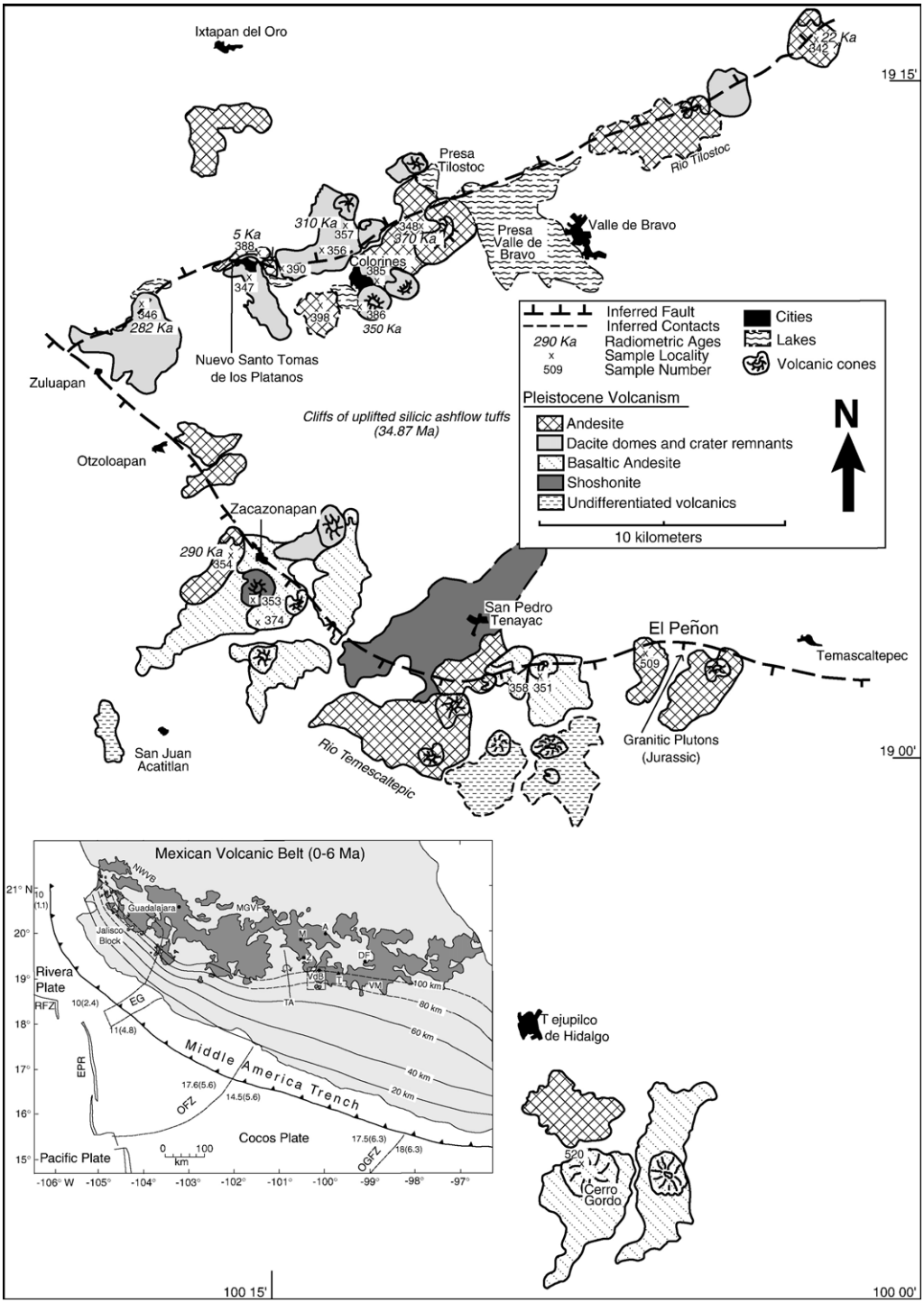

xenoliths were brought to the surface in a hornblende-bearing high-Mg andesite lava flow, and are themselves hornblende-bearing spinel lherzolite and chrome–olivine websterite, occuring in association with clinopyroxene megaxenocrysts. In addition, they have high oxygen fugacities, and show mineralogical evidence of modal metasomatism (Blatter and Carmichael, 1998). Quaternary in age (Blatter et al., 2001), the host lava flow was erupted along a fault escarpment located in the front of the MVB near El Peñon (Fig. 1). Here, we report the trace element and isotopic characteristics of these unique fragments of the upper mantle, and compare their compositional characteristics with those of the host rocks and xenoliths from other mantle domains in order to assess the processes operating in the mantle wedge and to ascertain the source of andesite magmas along active continental margins.

2. Background

The lithospheric mantle beneath El Peñon, Mexico, has been influenced by several subduction regimes. The earliest evidence for subduction is found in Permian granitic plutons of the East Mexico Arc that were emplaced into older basement when this region of central Mexico was part of the Gondwanan margin (Dickinson and Lawton, 2001, references therein). This subduction regime continued as the oceanic Mescalera Plate converged beneath the Del Sur block, forming the Middle Triassic Nazas arc (Dickinson and Lawton, 2001). During Middle Jurassic to Cretaceous times, subduction along this margin may have stalled as a new margin was created with the accretion of the Guerrero Superterrain from the west (Dickinson and Lawton, 2001). Arc-producing subduction resumed during the Cordilleran with the subduction of the Farallon Plate beneath the nearly assembled North American Plate. This regime produced the voluminous silicic ash flow tuffs exposed in the Sierra Madre Occidental (mountain range just north of the MVB) and in the El Peñon region. Sections of this material >1000 m thick are exposed in footwall cliff faces along normal faults near El Peñon. The current regime has involved subduction of the Cocos Plate beneath the North American Plate, which began in the Middle Miocene, following tectonic truncation of the continental margin (Karig et al., 1978), and initiated the present-day MVB (Fig. 1 inset). Cocos subduction continues along this margin at the rate of ~6 cm per year (DeMets et al., 1990). The front of the MVB arc has moved progressively toward the Middle America Trench over time (Hasenaka and Carmichael, 1985), presumably due to steepening of the slab angle. According to modeling by Pardo and Suarez (1995), the current arc-front (near El Peñon) lies approximately 80 km above the subducting Cocos slab.

The andesite flow that hosts the El Peñon xenoliths is part of a group of high-K and calc–alkaline basaltic andesites and andesites that erupted along the base of the escarpment of a large normal fault. Blatter and Carmichael (1998) argued that the presence of hornblende phenocrysts and complete absence of plagioclase phenocrysts in the host lava suggest equilibration with a high water content in excess of 8 wt.%. Phenocryst geothermometry, which yielded equilibration temperatures of 910 °C to 1055 °C, and generally high whole-rock Ni and Cr contents (57–196 ppm and 117–469 ppm, respectively) accompanied by high Mg# (67–75) for these andesites have been used to postulate that the host rocks were derived directly from the mantle (Blatter and Carmichael, 2001). This is supported by the presence of mantle peridotite xenoliths in at least one of the lava flows. The xenoliths are generally small (<2 cm), and are among the most oxidized mantle peridotites yet described (Δlog FMQ+1.5 to +2.4) (Blatter and Carmichael, 1998). The highly oxidized state of the xenoliths is consistent with high H_2O activity in the mantle wedge where the xenoliths originated. Their petrography, mineral elemental compositions and temperatures of equilibration can be found in Blatter and Carmichael (1998).

3. Results

We report trace element concentrations and Nd, Sr and Pb isotopic compositions, determined by a variety of methods identified in the data tables, for clinopyroxene and amphibole in some peridotite and websterite xenoliths, clinopyroxene megaxenocrysts and the host

Fig. 1. Volcanic deposits and sample localities in the Valle de Bravo region. The El Peñon flow is labeled in the middle right of the map where the sample Z-509 is indicated. The index map in the lower left corner shows the outline of the area shown labeled VdB. The index map shows the entire Mexican Volcanic Belt with volcanism from zero to six Ma shown in dark grey; modified after Pasquarè et al. (1991). The tectonic features are modified after Pardo and Suarez (1995). Abbreviations are: RFZ = Rivera Fracture Zone, EG = El Gordo Graben, EPR = East Pacific Rise, OFZ = Orozco Fracture Zone, OGFZ = O'Gorman Fracture Zone. The numbers along the Middle America Trench indicate the age of the subducting oceanic crust in million years (first number) and the convergence rate at that location in cm/yr (number in parenthesis); the black contours represent the depth to the subducted slab in km (Pardo and Suarez, 1995). Other abbreviations within the Mexican Volcanic Belt are NWVB = Northwest Volcanic Belt, MGVF = Michoacán–Guanajuato Volcanic Field (Hasenaka and Carmichael, 1985), M = Maravatío, A = Acambay, Z = Zitácuaro, VdB = Valle de Bravo, T = Nevado de Toluca, DF = Distrito Federal, VM = Valley of Mexico, and TA = Tzitzio Anticline.

Table 1
Trace element concentrations (ppm) for clinopyroxene and amphibole from xenoliths and phenocrysts from the host andesite lava

Sample #	X-4 (TS3)	X-4 (TS1)	X-4 (C1)	X-4 (C3)	X-12 (TS2)	X-12 (C1)	X-12 (C2)	X-14 (TS7)	X-14 (TS6)	X-14 (TS8)	X-14 (TS9)	X-6 (TS2)	X-6 (TS5)
Rock	Spinel lherzolite										Websterite		
Mineral	Clinopyroxene												
	Core	Rim	Core-to-rim	Core	Core	Rim	Core	Core	Rim	Core	Rim	Rim	Rim
La	0.2074	2.466	0.1493	0.0494	0.3791	1.312	0.0618	1.117	1.864	0.9828	2.203	1.782	1.929
Ce	0.6357	10.70	0.5434	0.3560	1.1613	5.216	0.3990	2.848	8.053	2.601	9.597	7.020	8.454
Nd	0.6317	10.50	0.7865	0.5546	0.9289	6.060	0.5714	1.589	8.253	1.498	10.34	8.260	8.669
Sm	0.3734	3.063	0.3991	0.3765	0.4082	1.775	0.3583	0.7205	2.580	0.6933	3.098	2.455	2.629
Eu	0.1322	1.050	0.1950	0.1382	0.1565	0.7316	0.1057	0.2706	0.8782	0.2816	1.146	0.9212	1.018
Dy	0.3954	2.934	0.7503	0.4713	0.5804	2.018	0.4122	1.147	2.146	1.198	3.129	2.235	2.547
Er	0.3108	1.591	0.3900	0.4074	0.4146	0.8791	0.2580	0.9023	1.328	0.7807	1.624	1.177	1.463
Yb	0.2845	1.496	0.4224	0.2979	0.3770	0.8838	0.2830	0.7090	1.213	0.7998	1.532	1.165	1.181
Sr	4.770	117.3	92.37	5.504	34.68	146.4	5.244	26.63	113.3	24.73	97.52	138.4	104.5
Zr	3.021	25.17	14.48	2.970	5.974	30.14	2.271	13.24	30.35	11.86	20.56	24.99	13.97
Ti	603.5	2817	2086	781.0	3730	3574	745.2	924.3	3462	922.2	2723	3013	2084
Y	1.984	13.68	10.55	1.981	19.03	16.59	2.105	7.390	16.09	7.532	15.15	16.10	10.44
V	84.06	227.3	204.8	111.5	478.2	287.7	99.45	132.3	257.8	136.1	254.0	262.5	181.3
Cr	1763	759.4	2212	1085	7628	665.2	1326	2992	1340	2968	1281	1596	919.7

Sample #	X-4 (TS4)	X-4 (TS2)	X-4 (C2)	X-12 (TS1)	X-12 (TS3)	X-14 (TS1)	X-14 (TS2)	X-6 (TS1)
Rock	Spinel lherzolite						Websterite	
Mineral	Amphibole							
	Core	Rim	Rim	Core	Core	Rim	Rim	Rim
La	0.9465	3.661	3.547	0.4045	0.2750	3.615	3.200	2.681
Ce	3.804	15.99	15.80	2.109	1.787	16.99	14.46	11.92
Nd	3.213	15.00	16.65	2.832	2.820	16.41	15.42	12.26
Sm	1.075	4.066	3.609	1.179	1.348	4.781	3.676	3.699
Eu	0.5880	1.667	2.118	0.6828	0.7292	2.022	2.115	1.684
Dy	2.069	4.632	4.814	2.662	2.705	4.589	4.956	3.805
Er	1.250	2.195	2.552	1.606	1.780	2.431	2.670	2.272
Yb	1.229	2.139	2.662	1.779	1.783	2.461	3.341	1.955
Sr	42.53	452.0	546.7	4.393	84.08	529.8	443.4	515.6
Zr	7.263	52.34	55.19	3.110	8.474	39.50	38.94	51.14
Ti	3813	14276	14619	678.1	2790	15026	15264	16717
Y	22.12	29.53	26.53	2.398	18.26	25.97	25.78	33.02
V	472.6	484.1	506.3	99.78	374.7	498.3	564.5	538.0
Cr	10054	1950	216.1	1531	9049	831.2	392.5	737.0

Sample #	X-10 (TS2)	X-10 (TS1)	X-14 (TS1)	X-14 (TS2)	X-14 (TS3)	X-14 (TS4)	X-16 (TS1)	X-16 (TS2)
Rock	Phenocrysts							
Mineral	Clinopyroxene					Amphibole	Clinopyroxene	
	Core	Rim	Core	Core	Rim	Core	Core	Core
La	2.779	1.312	1.977	1.465	1.733	2.919	3.569	2.765
Ce	8.677	5.490	8.853	6.064	8.085	14.17	11.31	8.284
Nd	4.743	5.003	8.862	7.335	9.354	14.95	7.520	5.091
Sm	1.023	1.483	2.397	2.474	3.161	5.208	2.535	1.988
Eu	0.3170	0.5265	0.8753	0.8476	1.005	2.275	0.5725	0.4388
Dy	0.8283	1.436	2.230	1.934	2.551	5.280	1.530	1.320
Er	0.3889	0.6420	1.022	1.007	1.272	2.667	0.7455	0.6457
Yb	0.3451	0.7336	1.180	0.9793	1.185	2.476	0.8760	0.6464
Sr	61.67	140.3	91.05	107.6	85.66	508.3	65.94	63.74
Zr	46.75	10.55	70.40	18.64	12.16	31.59	46.07	40.63

Table 1 (*continued*)

Sample #	X-10 (TS2)	X-10 (TS1)	X-14 (TS1)	X-14 (TS2)	X-14 (TS3)	X-14 (TS4)	X-16 (TS1)	X-16 (TS2)
Rock	Phenocrysts							
Mineral	Clinopyroxene					Amphibole	Clinopyroxene	
	Core	Rim	Core	Core	Rim	Core	Core	Core
Ti	2619	1693	7073	3287	1574	12762	2831	2570
Y	6.681	7.612	44.08	12.52	11.18	26.94	7.050	6.290
V	348.9	165.5	479.5	299.3	158.4	460.2	376.9	365.1
Cr	444.6	3196	619.6	1397	789.2	947.0	318.7	242.5

Note: TS: measurements were performed on polished thin sections; C: measurements were made on rock chips.

andesite and related lavas (Tables 1–3, and Figs. 2–6). Trace element concentrations for the peridotite minerals (clinopyroxene and amphibole) and megaxenocrysts either in thin section, polished rock chips or grain mounts, have been determined by ion microprobe analysis on a Cameca 3f at the Woods Hole Oceanographic Institution (WHOI) using the methods described by Shimizu et al. (1978), and Shimizu and Le Roex (1986), and for the host andesite and associated lava flows, on whole-rock powders by ICP-MS at Washington State University. Sample sizes for the ultramafic xenoliths were too small for conventional isotopic work. Diopside in a single peridotite sample was analyzed experimentally for its Pb isotopic compositions using a Cameca 1270 large-radius ion microprobe, with mixed success as described below. However, Nd–Sr–Pb isotopic compositions were determined for the clinopyroxene megaxenocrysts, the andesite host rock and related lavas by thermal ionization mass spectrometry at the University of Michigan using methods described elsewhere by Mukasa et al. (1987, 1991) and Mukasa and Shervais (1999).

3.1. Trace element results

We measured the trace element concentrations of clinopyroxene and amphibole (when present) in the peridotite xenoliths, focusing chiefly on the grain cores. In a few samples we analyzed the rims as well to document reaction effects. It was not always possible to obtain data from a rim and a core in the same grain owing, in most cases, to one or the other of these zones being smaller than the oxygen beam in the ion microprobe. Wide, optically clear cores tended to have thin rims and offered the best targets for analysis. The infrequent large rims were analyzed opportunistically, and because their trace element abundance patterns were found to be similar to those of the cores, rim analysis became only a very small component of our overall study. We also measured trace element concentrations of clinopyroxene and amphibole in the coarse rinds that encapsulate the xenoliths and separate them from the host lava. Rare earth element (REE) abundances for clinopyroxene (diopside) in the peridotites, normalized to primitive mantle (PM) values of McDonough and Sun (1995), cover a wide range, especially for the light (L) REE (Table 1 and Fig. 2A). Diopside La shows variations of one order of magnitude in the xenolith suite, from a highly depleted convex pattern with a La_N/Sm_N value of 0.09 for an amphibole-bearing lherzolite (sample X-4, core C3) to a nearly flat pattern at $\sim 1.5 \times$ PM with a La_N/Sm_N value of 1.00 in an amphibole-free lherzolite (sample X-14). Diopside in sample X-14 has a negative inflection at Nd, possible only if the overall REE pattern is not a primary feature of the rock. Clinopyroxene (augite) in the coarse rind that surrounds each xenolith has a convex pattern with the middle (M)REE higher than both the LREE and heavy (H)REE (Fig. 2A). This characteristic is shared by augite and amphibole phenocrysts in the host lava (X-14 samples, Fig. 2B), though the amphibole generally has higher REE concentrations, except for La. Strontium, Zr, Ti, Y and V are significantly less abundant in the peridotite clinopyroxene (except for one grain each in samples X-4 and X-12) than they are in the rind and lava phenocrysts (Table 1). Although the rind and lava clinopyroxene phenocrysts have similar concentrations for these trace elements, coherence of the resulting patterns for the rind clinopyroxene and lack of it in the lava phenocrysts is a conspicuous difference. Two augite megaxenocrysts (X-10 and X-16) have REE patterns similar to those of the augite phenocrysts in the host lava and the rind separating the peridotite xenoliths from the lava (Fig. 2B). Megaxenocryst X-16 has an LREE-enriched pattern with no significant variation between the crystal's core and rim while X-10 has a convex REE pattern for the core and an LREE-enriched pattern for the rim. Overall, the trace element patterns for the megaxenocrysts are distinctly different from those of the Cr-diopside grains in the peridotite xenoliths.

Table 2
Trace element concentrations (ppm) of the host andesite, associated lavas (prefix: z), and peridotite xenoliths (prefix: x)

Sample #	Z-342	Z-346	Z-348	Z-351	Z-353	Z-354	Z-356	Z-357	Z-358	Z-374	Z-385	Z-386	Z-388	Z-390	Z-509	Z-520	X-4	X-12	X-30	X-33	X-45
La	13.73	12.40	12.86	112.40	55.92	13.26	13.96	16.47	21.07	22.34	23.73	15.57	14.58	15.73	25.27	18.29	17.61	13.32	2.33	2.80	5.51
Ce	27.14	24.43	24.83	128.89	109.2	27.15	27.96	32.69	30.81	44.55	32.44	28.66	28.19	31.04	46.90	37.19	12.94	11.88	6.15	8.02	16.61
Pr	3.32	3.12	3.03	21.31	13.85	3.44	3.49	3.99	4.27	5.52	5.00	3.72	3.45	3.75	6.14	4.76	3.48	2.93	0.96	0.81	1.47
Nd	13.96	13.31	12.74	91.60	58.66	15.01	14.85	16.67	18.54	23.33	20.52	15.68	14.48	15.67	25.26	20.20	14.90	12.82	4.86	3.44	6.62
Sm	3.27	3.14	3.21	17.54	11.76	3.62	3.48	3.59	4.21	4.98	4.42	3.55	3.18	3.50	5.32	4.58	2.77	2.64	1.50	0.73	1.46
Eu	1.08	1.05	1.04	5.08	3.22	1.16	1.10	1.12	1.42	1.58	1.24	1.12	1.07	1.11	1.65	1.44	0.96	0.89	0.45	0.18	0.47
Gd	2.96	2.85	3.19	15.50	8.54	3.18	3.24	3.05	4.42	4.20	4.00	3.33	2.88	3.02	4.44	4.02	2.98	2.66	1.54	0.70	1.35
Tb	0.454	0.431	0.515	2.08	1.12	0.496	0.511	0.452	0.688	0.631	0.596	0.522	0.430	0.454	0.657	0.618	0.44	0.41	0.25	0.11	0.20
Dy	2.54	2.46	3.06	11.00	5.35	2.79	3.04	2.48	4.05	3.43	3.13	2.90	2.37	2.47	3.81	3.61	2.66	2.51	1.49	0.73	1.18
Ho	0.479	0.473	0.618	2.11	0.943	0.562	0.589	0.470	0.837	0.648	0.592	0.562	0.440	0.471	0.765	0.715	0.54	0.52	0.29	0.15	0.24
Er	1.23	1.25	1.66	5.15	2.18	1.45	1.62	1.22	2.25	1.66	1.53	1.49	1.15	1.22	2.04	1.91	1.44	1.39	0.76	0.44	0.65
Tm	0.178	0.182	0.250	0.69	0.303	0.209	0.230	0.178	0.321	0.243	0.223	0.221	0.170	0.181	0.283	0.259	0.20	0.19	0.11	0.07	0.09
Yb	1.11	1.12	1.56	3.93	1.93	1.27	1.45	1.11	1.91	1.45	1.28	1.34	1.06	1.13	1.73	1.67	1.19	1.20	0.65	0.42	0.60
Lu	0.175	0.176	0.245	0.58	0.299	0.192	0.218	0.171	0.297	0.224	0.202	0.211	0.158	0.177	0.279	0.260	0.19	0.19	0.10	0.07	0.10
Cs	13.98	13.95	17.08	0.88	22.22	13.52	16.78	11.75	24.13	22.93	12.87	13.27	12.61	12.18	18.67	25.98	0.06	0.13	0.17	0.12	0.06
Rb	28.80	22.77	34.99	21.40	31.65	29.18	28.79	29.64	25.75	18.43	30.60	25.89	27.49	29.92	31.91	21.72	0.6	1.5	1.4	1.5	0.6
Ba	405	376	385	656	1056	391	375	404	398	452	394	383	406	387	425	351	42	51	28	17	35
Th	2.38	2.02	2.91	3.86	5.21	3.47	3.31	3.27	2.65	2.86	3.08	3.15	2.50	2.98	3.59	2.83	0.08	0.24	0.16	0.03	0.03
U	0.695	0.620	0.927	1.12	1.52	0.905	0.904	0.860	0.905	0.891	0.848	0.860	0.770	0.785	1.09	0.871	0.13	0.13	0.10	0.10	0.16
Nb	3.73	2.83	3.42	4.52	5.52	3.28	3.77	4.12	3.55	4.28	4.03	3.78	3.73	3.93	4.53	3.39	0.22	0.48	0.25	0.09	0.08
Ta	0.259	0.205	0.273	0.29	0.318	0.259	0.274	0.282	0.252	0.273	0.292	0.277	0.254	0.279	0.318	0.224	0.01	0.03	0.02	0.00	0.01
Pb	5.90	4.85	6.53	7.41	10.42	5.89	5.67	6.31	5.96	4.77	6.04	6.05	6.43	5.76	6.17	5.36	0.60	1.70	1.03	0.42	0.55
Sr	677	882	547	1225	1451	851	781	996	642	844	809	731	742	918	1265	642	49	114	101	24	34
Zr	129	100	125	110	152	124	129	126	98	130	132	136	130	135	159	129	8	17	16	2	3
Hf	3.34	2.93	3.51	3.35	4.36	3.65	3.43	3.60	2.55	3.23	3.54	3.57	3.30	3.57	4.37	3.24	0.25	0.52	0.57	0.07	0.12
Y	12.80	12.91	16.42	57.70	25.16	14.38	15.76	13.13	28.75	17.59	16.33	15.30	12.11	13.19	23.19	19.78	20.01	17.92	8.37	4.61	8.97
Sc	13.98	13.95	17.08	25.10	22.22	13.52	16.78	11.75	24.13	22.93	12.87	13.27	12.61	12.18	18.67	25.98	27.8	25.8	46.8	9.0	14.1
V	131	100	93	149	180	90	119	94	134	163	111	82	108	97	143	187	NA	NA	NA	NA	NA
Cr	170	111	144	504	246	22	170	128	289	491	154	142	257	144	117	469	NA	NA	NA	NA	NA
Ni	57	73	59	265	155	25	57	104	146	220	82	89	176	96	60	196	NA	NA	NA	NA	NA

Note: All analyses but Zr, V, Cr, and Ni were conducted by the ICP-MS method; Zr, V, Cr, and Ni concentrations were obtained by the XRF method.

Table 3
Isotope compositions of Mexican clinopyroxene megacrysts and bulk rock basaltic andesites and andesites

Sample #	Sm (ppm)	Nd (ppm)	Rb (ppm)	Sr (ppm)	Pb (ppm)	U (ppm)	$^{147}Sm/^{144}Nd$	$^{143}Nd/^{144}Nd$	$^{87}Rb/^{86}Sr$	$^{87}Sr/^{86}Sr$	$^{206}Pb/^{204}Pb$	$^{207}Pb/^{204}Pb$	$^{208}Pb/^{204}Pb$	$^{238}U/^{204}Pb$
Megacrysts														
X-10	2.505	9.311	1.566	142.8	0.415	0.132	0.16264	0.512858±23	0.0316	0.703643±22	18.611	15.578	38.181	20.313
X-16	2.004	7.120	0.729	87.2	0.508	0.085	0.17012	0.512833±21	0.0241	0.703390±18	18.624	15.565	38.191	10.682
Andesites														
Z-342	2.565	12.218	24.952	619.8	5.649	0.641	0.12692	0.512824±23	0.1159	0.703809±17	18.586	15.547	38.252	7.200
Z-351	5.152	37.732	18.019	1159	6.809	n.d.	0.11232	0.512902±23	0.0447	0.703626±22	18.651	15.570	38.387	n.d.
Z-353	8.634	54.606	25.121	1333	8.733	1.353	0.11590	0.512857±21	0.0542	0.704435±18	18.688	15.585	38.442	9.869
Z-509	4.799	18.965	23.800	1115	5.348	0.764	0.12117	0.512909±24	0.0675	0.703376±18	18.606	15.567	38.312	9.073
Z-520	5.864	18.189	17.401	582.1	5.584	0.718	0.12843	0.512915±22	0.0891	0.704052±21	18.627	15.549	38.295	8.167

Note: Errors for the Nd and Sr isotopic compositions are two sigma.

Similar to the clinopyroxene, amphibole within the peridotite xenoliths has a convex pattern with depleted LREE and a La_N/Sm_N value of 0.13 (Fig. 2C). The higher concentration of all the REE in amphibole compared to clinopyroxene for any peridotite sample is consistent with differences in partition coefficients for the two minerals (Fujimaki et al., 1984; Chazot et al., 1996; Zack et al., 1997). Amphibole phenocrysts in the rinds around the peridotite xenoliths also have convex normalized REE patterns, but with MREE higher than LREE and HREE and La_N/Sm_N of ~0.56. Concentrations for the trace elements Sr, Zr, Ti, Y and V are also lower in the peridotite xenolith amphibole than they are in the rind and host lava amphibole phenocrysts. Chromium, however, is higher in the peridotite xenolith amphibole, consistent with the suggestion of Blatter and Carmichael (1998) that this amphibole is a metasomatic replacement product of diopside and orthopyroxene.

Primitive mantle-normalized trace element abundances for the host lava (Z-509) and fourteen volcanic samples related to the host lava (Table 2 and Fig. 3) show remarkable uniformity (with La_N/Yb_N = 5.6–12.7) in spite of their large range in SiO_2 (52.05–64.50 wt.%) and MgO (2.80–9.09 wt.%). The one exception (Z-353) is the sample with the lowest SiO_2 (52.05%) and high MgO (6.61%), which has considerably higher concentrations of the LREE and MREE as well as Ba, Th, and U compared to the rest of the samples. All of the lavas analyzed exhibit high concentrations of Ba and Sr and negative anomalies for the high field strength elements (HFSE) – *i.e.*, elements with a high charge to ionic radius ratio – such as Nb, Ta and Hf, typical of arc magmas.

3.2. Radiogenic isotope results

Isotopic compositions of Sr, Nd and Pb are reported for five basaltic andesite and andesite samples including the host lava, and two clinopyroxene megaxenocrysts (Table 3 and Figs. 4 and 5). These are compared with basalts in the Basin and Range and Rio Grande Rift tectonic provinces (Arizona, California, New Mexico and northern Mexico) (Roden et al., 1988; Galer and O'Nions, 1989; Nimz et al., 1993, 1995), and also with lavas from the western and central MVB (Verma and Nelson, 1989; Wallace and Carmichael, 1994; Luhr and Aranda-Gomez, 1997; Verma, 1999; Chesley et al., 2002; Petrone et al., 2003). The host lavas have $^{87}Sr/^{86}Sr$ values with a range of 0.703376±18 to 0.704435±18, $^{143}Nd/^{144}Nd$ of 0.512824±23 to 0.512915±22, $^{206}Pb/^{204}Pb$ of 18.563 to 18.641, $^{207}Pb/^{204}Pb$ of 15.536 to 15.619, and $^{208}Pb/^{204}Pb$ of 38.053 to 38.242 (Table 3). On the $^{143}Nd/^{144}Nd$ *versus* $^{87}Sr/^{86}Sr$ diagram

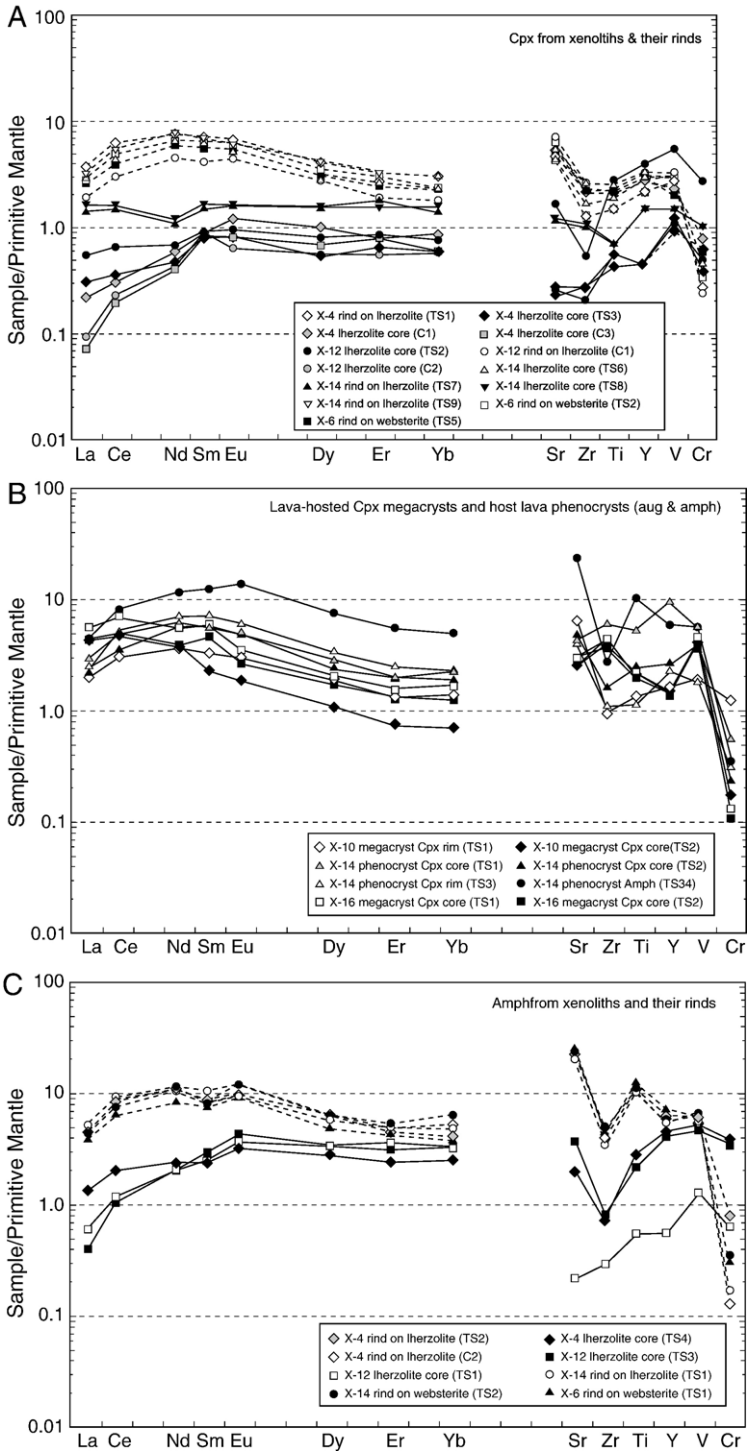

Fig. 2. Primitive mantle-normalized element distribution patterns determined *in-situ* by ion microprobe for (A) clinopyroxene within the xenolith and from the rind encapsulating the xenolith, (B) lava-hosted clinopyroxene megaxenocrysts and host lava augite and amphibole phenocrysts, and (C) amphibole from the xenoliths and their rinds. Note the comparison between cores and rims in the clinopyroxene grains. Normalization values are from Sun and McDonough (1989).

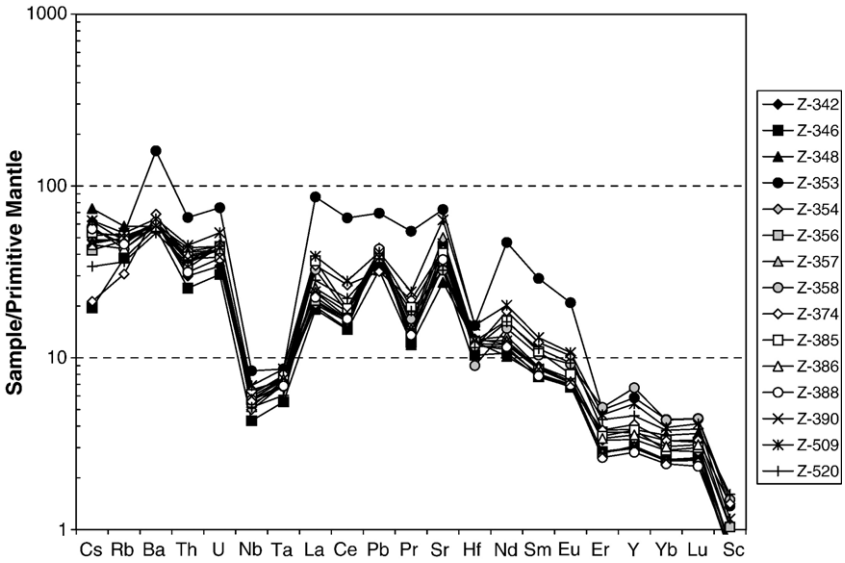

Fig. 3. Primitive mantle-normalized element distribution patterns for the El Peñon high-Mg siliceous andesites determined by ICP-MS. Note the distinctive negative anomalies for Nb, Ta and Hf and positive anomalies for Ba, Pb and Sr, all characteristic of subduction-zone magmas. Normalization values are from Sun and McDonough (1989). See text for discussion.

(Fig. 4), the analyzed Mexican andesites fall either in or close to the field for Quaternary lavas from of the western and central MVB (Verma and Nelson, 1989; Wallace and Carmichael, 1994; Luhr and Aranda-Gomez, 1997; Verma, 1999; Righter, 2000; Chesley et al., 2002; Petrone et al., 2003). Clinopyroxene megaxenocrysts (X-10 and X-16; Table 3, Fig. 4) have ratios similar to those of the lavas. On Pb co-variation diagrams (Fig. 5), the host rocks fall either within or just outside the field for East Pacific Rise

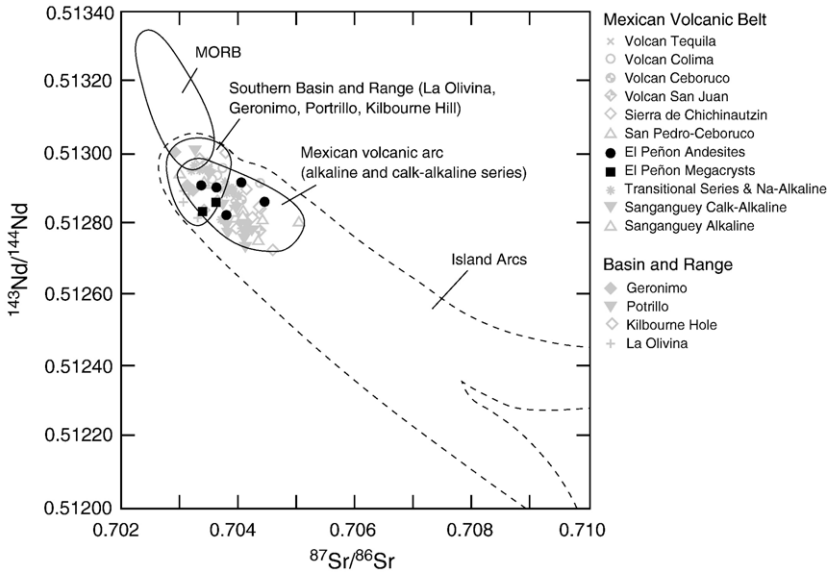

Fig. 4. $^{143}Nd/^{144}Nd$ *vs* $^{87}Sr/^{86}Sr$ covariation diagram comparing the El Peñon andesite samples and clinopyroxene megaxenocrysts (dark symbols) to literature data for the Mexican Volcanic Belt (Verma and Nelson, 1989; Wallace and Carmichael, 1994; Verma, 1999; Petrone et al., 2003), southern Basin and Range tectonic province (Roden et al., 1988; Nimz et al., 1995), mid-ocean ridge basalts (MORB) (Hofmann, 1997), and island arcs (Wilson, 1989). See text for discussion.

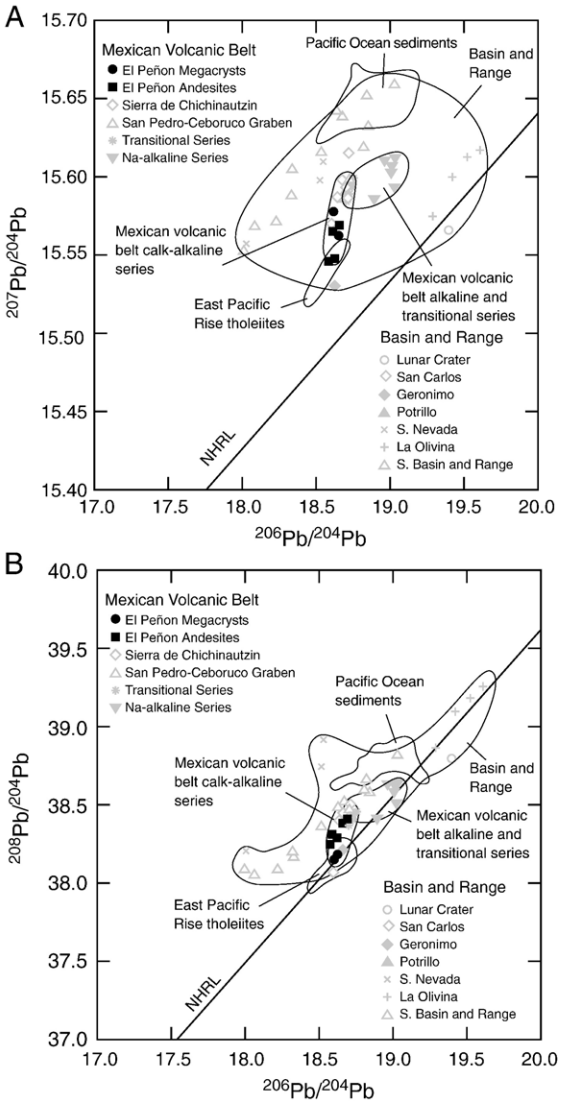

Fig. 5. (A) $^{207}Pb/^{204}Pb$ *vs* $^{206}Pb/^{204}Pb$ and (B) $^{208}Pb/^{204}Pb$ *vs* $^{206}Pb/^{204}Pb$ covariation diagrams with the El Peñon andesite and clinopyroxene megaxenocryst data (dark symbols) compared to lavas from other localities in the Mexican Volcanic Belt (MVB) and Basin and Range tectonic province. Data sources are the same as in Fig. 4. NHRL = northern hemisphere reference line (Hart, 1984); the East Pacific Rise data are from Smith (1999); and data for Pacific Ocean sediments are from Church and Tatsumoto (1975) and Plank and Langmuir (1998).

MORB tholeiites. These values are very similar to those of the two clinopyroxene megaxenocrysts we have analyzed and to those of western and central Mexico volcanoes (Wallace and Carmichael, 1994; Verma, 1999) in the same arc. The lavas and megaxenocrysts exhibit a much narrower range in isotopic compositions compared to the basaltic volcanism in the Basin and Range Province in northern Mexico and southwestern US (Roden et al., 1988; Galer and O'Nions, 1989; Nimz et al., 1993, 1995).

While the peridotite xenoliths are too small to be analyzed by conventional thermal ionization mass spectrometry, one clinopyroxene grain from a peridotite xenolith (X-14) was measured experimentally on a Cameca 1270 large-radius ion microprobe at WHOI for its $^{208}Pb/^{206}Pb$ and $^{207}Pb/^{206}Pb$ values. Several test spots on augite phenocrysts in the host andesite and Cr-diopside in peridotite xenolith X-14 conducted with a high current primary beam (35nA) and 3500MRP (mass resolution power) failed to generate more than 10 counts per second (cps) for ^{208}Pb on the ion microprobe. Analysis of a single Cr-diopside spot in peridotite xenolith X-14, however, appears to have fortuitously sampled a Pb-rich mineral inclusion, giving an average count rate of 42 cps. Measurements over a one-hour period in this high-count spot yielded $^{208}Pb/^{206}Pb$ and $^{207}Pb/^{206}Pb$ values of 2.051 ± 0.021 (1σ) and 0.843 ± 0.010 (1σ), respectively. These plot in the Pacific MORB field on the $^{208}Pb/^{206}Pb$ *versus* $^{207}Pb/^{206}Pb$ covariation diagram (not reproduced here), and are within error, indistinguishable from the Pb isotopic ratios determined by TIMS for megaxenocrysts X-10 and X-16 ($^{208}Pb/^{206}Pb = 2.0516 \pm 0.0001$ and 2.0505 ± 0.0001; $^{207}Pb/^{206}Pb = 0.8370 \pm 0.0001$ and 0.8357 ± 0.0001, respectively).

4. Discussion

4.1. Melt depletion and metasomatism of the upper mantle

The wide range in LREE abundances for clinopyroxene in the peridotite xenoliths (Fig. 2A) could be interpreted to represent any of three possibilities. One is that the range resulted from different degrees of melting and melt extraction from the mantle source regions for each of the xenolith samples before they were entrained. Secondly, it is conceivable that these patterns are the result of exchange reactions between peridotite xenoliths and their host lavas during entrainment and transport to the surface. And thirdly, there is the possibility that the patterns are due to differential *in situ* metasomatism of peridotites depleted previously in LILE and basaltic components by melt extraction events.

Developing the REE patterns observed in clinopyroxene by removing different amounts of melt from each of the peridotite samples may not be the best explanation in this case because the REE abundances do not correlate with CaO and Al_2O_3, two basaltic components that would be expected to decrease in concentration within the peridotite as more melt is removed (*e.g.* Klein and Langmuir, 1987). (Electron microprobe data for minerals in these xenoliths can be found in Table 1 of Blatter and

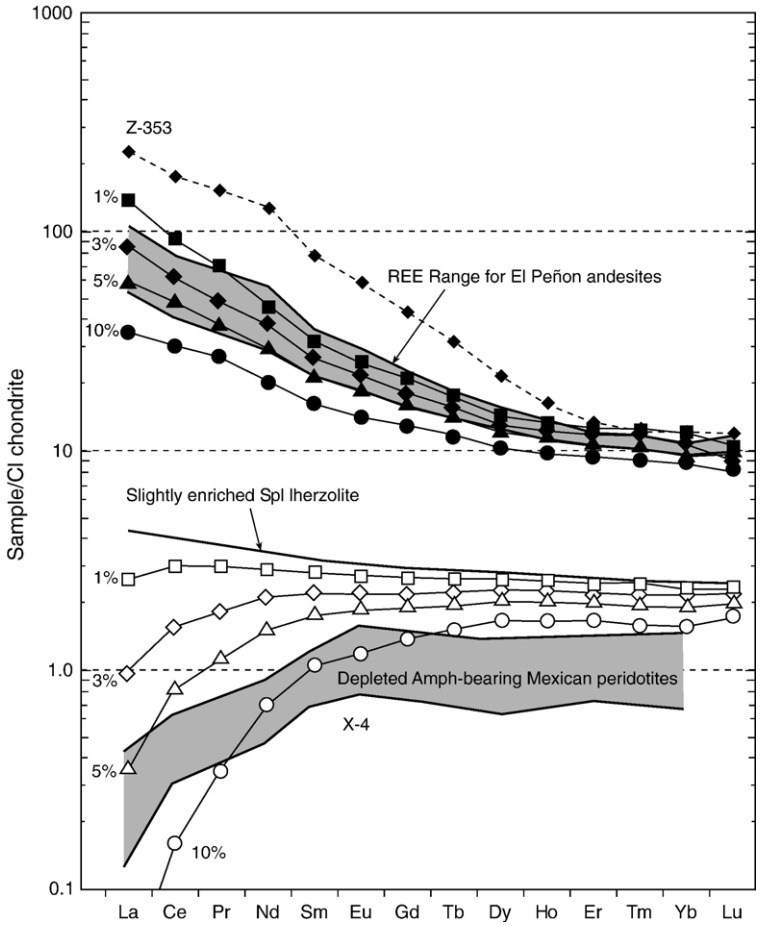

Fig. 6. Illustration of the results of the calculations for 1, 3, 5 and 10% partial melting of a slightly enriched spinel lherzolite. The top half of the diagram shows the REE abundance patterns of magmas derived by different degrees of partial melting (thin black lines) of this material. The shaded area outlined by the bold black lines in the top half of the diagram shows the compositional range of the 15 high-Mg siliceous andesites analyzed. The bottom half of the diagram shows the elemental patterns resulting from successive depletion of the residual rock with increasing degree of partial melting. Note that there is no perfect match between any of the calculated residue compositions and estimated compositions for the Mexican peridotite xenoliths studied.

Carmichael (1998) and are not reproduced here). Moreover, sample X-14 with the highest concentration of LREE has an inflection or negative anomaly at Nd, which is difficult to explain by melting processes given that partition coefficients would favor preferential removal of La and Ce over Nd. It could also be argued that preservation of materials with primitive mantle geochemical characteristics – presumably to become the sources of Quaternary Mexican volcanism – is not likely in an area that has had sustained plate convergence since possibly the Permian (Dickinson and Lawton, 2001).

The possibility that the observed REE patterns in the peridotite clinopyroxene are the result of reaction between the xenoliths and their host rocks during transit to the surface is also considered to be weak for three reasons. First, dissolution experiments by Scarfe and Brearley (1987) demonstrated that peridotite xenoliths of El Peñon size survive in their host magmas for only a matter of hours. Their preservation therefore requires delivery to the surface at speeds much faster than would be conducive to significant ionic diffusion during exchange reactions. For the El Peñon peridotite xenoliths, there is also evidence that a protective rind of coarse augite and hornblende encapsulated these inclusions at mantle conditions thus preventing the possibility of reaction with the host magmas (Blatter and Carmichael, 1998). Supporting these arguments is the fact that the amphibole and clinopyroxene within the peridotite xenoliths are different in composition from those found in the encapsulating rind and in the host El Peñon andesite. In other words, if the amphibole in the peridotite had grown during transport to the surface by the andesite

magma, we would expect it to have a composition similar to that of the amphiboles in the rind and in the lava.

Pre-entrainment metasomatism imposed on peridotite previously depleted in incompatible elements by melt extraction appears to be the most viable model for the observed REE patterns. This process explains the occurrence of multiple generations of Cr-rich amphibole replacing pyroxenes, and magnetite and hematite in place of spinel. It also offers explanations for the inflection at Nd in the REE patterns for sample X-14 (Fig. 2A), grain-to-grain differences in elemental abundances within the same xenolith sample, and the differences in composition between the peridotite and host rock amphibole and clinopyroxene. As the thermometry and phase equilibria evidence indicate entrainment at mantle conditions, it follows that the peridotites must have been metasomatized in some earlier events at mantle conditions, not while entrained by the host magma during transit to the surface.

In spite of significant amounts of amphibole in two of the three peridotite xenoliths (3–8 modal percent) (please see Table 1 of Blatter and Carmichael (1998) for details), a record of melt extraction indicated by LREE depletion remains quite evident in these rocks. There is no correlation between amphibole modal abundance and level of LREE depletion or enrichment in the peridotite minerals. For example, sample X-12 with 8 modal percent amphibole has a mixed population of clinopyroxene grains with a wide range in LREE abundances. Moreover, amphibole in X-12 has lower LREE concentrations compared to amphibole in sample X-4 with only 3 modal percent. Variations in LREE concentrations between clinopyroxene grains in the same sample are an important discovery in these rocks, which are direct representatives of the mantle wedge above an active subduction zone. Modeling of metasomatism in the upper mantle has usually invoked continuous porous flow of fluids or magma through the solid rock (Navon and Stolper, 1987; Bodinier et al., 1990; Kelemen et al., 1992; Sen et al., 1993), which is envisioned to induce progressive change in chemical compositions by pervasive chromatographic effects on all grains. However, the grain-to-grain differences in LREE concentrations documented for these Mexican xenoliths indicate that fluid or magma transport through the upper mantle can be channelized, and in so doing, metasomatizing some grains more intensively than others.

The process by which metasomatic components are introduced into mantle rocks continues to generate vigorous debate (Ulmer and Trommsdorff, 1995; Iwamori, 2000; Kerrick and Connolly, 2001a,b; Peacock, 2001). For these Mexican xenolith samples, the level of LREE enrichment is not correlated with the modal abundances of Cr-diopside or the basaltic components (Al_2O_3 and CaO) in the mineral. This suggests that metasomatism was most likely accomplished by introduction of aqueous fluids rather than silicate melts. The experimental work of Aizawa et al. (1999) demonstrated that subsolidus dehydration of chlorite and phengitic muscovite in subducted sediments – rather than partial melting – is the dominant process in the introduction of the sediment component into the mantle wedge. Sediment-derived fluids are very effective in transporting some trace elements (LILE and LREE, in particular). Aizawa et al.'s work showed that Sr is highly mobile, and is, therefore, one of the most easily transported elements during sediment dehydration. This mobility might explain the rather high concentrations in the El Peñon andesites of Sr and consequently high Sr/Y values, which are comparable to those of slab-derived adakite lavas (Kepezhinskas et al., 1995; Rapp et al., 1999; McInnes et al., 2001).

High concentrations of Cr in the peridotite amphibole, as documented previously by Blatter and Carmichael (1998), indeed support the conclusion that metasomatism hydrated the already Cr-rich pyroxenes of the peridotite without the introduction of new silicate minerals. Whatever the fluid source, the extremely high oxygen fugacity for the El Peñon xenoliths supports the notion that fluid migration through the mantle wedge was facilitated by hydrofracturing (McInnes et al., 2001). Ascent of H_2O-rich fluid through these mantle fractures can create a network of oxidized channels with metasomatized peridotite enriched in orthopyroxene, clinopyroxene, phlogopite, amphibole, magnetite and Fe–Ni sulphides, very much like the El Peñon xenoliths we report on here.

4.2. Comparison of the El Peñon xenoliths with other mantle xenoliths

The most relevant mantle xenoliths to compare with the El Peñon xenoliths include those from the following localities: (1) Quaternary volcanic fields of the southern Basin and Range Province — Sierra Madre Occidental and Mesa Central tectonic provinces of central Mexico (Luhr and Aranda-Gomez, 1997), and ~2-Ma basanitic cinder at La Olivina in north central Mexico (Nimz et al., 1995), (2) Late Tertiary to Quaternary volcanic fields of the southwestern United States (Roden et al., 1988; Wilshire et al., 1988; Galer and O'Nions, 1989), and (3) other magmatic arcs with xenoliths brought to the surface by andesite (Tanaka and Aoki, 1981; Conrad and

Kay, 1984; Maury et al., 1992; Parkinson and Arculus, 1999). Data available permit us to compare only oxygen fugacities and rare earth element abundance patterns; radiogenic isotope data for peridotite xenoliths in arc settings are still too limited in number for meaningful comparisons.

Blatter and Carmichael (1998) showed that the El Peñon xenoliths are the most oxidized mantle peridotites yet described (Δlog FMQ + 1.5 to + 2.4). Samples from Kilbourne Hole, New Mexico and San Carlos, Arizona, two localities representing the Late Tertiary to Quaternary volcanic fields of the southwestern United States, have a range that spans from 1.7 log units below to 1 log unit above FMQ, overlapping with the field for MORB and the abyssal peridotite array (Wood and Virgo, 1989; Parkinson and Arculus, 1999). Closer to El Peñon, xenoliths from the Tepehuano tectonic terrane of the Sierra Madre Occidental Mountains, just north of the MVB, have oxygen fugacities that increase from southeast to northwest between − 1.3 and + 0.3 log units relative to FMQ (Luhr and Aranda-Gomez, 1997). This systematic increase is correlated with distance from a paleosubduction zone, with samples originating closest to the Mesozoic–Cenozoic paleo-trench being the most strongly overprinted by slab-derived, oxidizing fluids. The broader survey of oxygen fugacities in arc spinel peridotites from Ichinomegata (Japan), Marelava (Vanuatu), Grenada, Marianas, Solomon Islands and Simcoe (Cascade arc, Washington) done by Parkinson and Arculus (1999) yielded a range of + 0.3 to + 2.0 relative to the FMQ buffer. Only the Marelava peridotites approach – though do not exceed – the values for the El Peñon xenoliths.

REE abundance patterns for peridotites in the southern Basin and Range province are largely based on whole-rock analyses, which means that direct comparisons with the El Peñon data obtained on individual minerals (amphibole and clinopyroxene) is not possible. Nevertheless, some useful generalities can be made, such as the observation that most peridotites in the area (*e.g.*, Kilbourne Hole, La Olivina and Sierra Madre Occidental) have chondrite-normalized patterns dominated by light REE depletion (Roden et al., 1988; Nimz et al., 1995; Luhr and Aranda-Gomez, 1997), attributable to varying degrees of melt extraction. There are a few samples at each of these localities that exhibit patterns of LREE enrichment, probably because of metasomatism driven largely by subduction processes. As argued elsewhere in the text, a history of depletion and metasomatism is envisioned for the El Peñon mantle xenoliths as well.

4.3. Andesite as a direct mantle melt? The trace element perspective

The association between andesite and peridotite xenoliths is very unusual, but seems to support the idea that andesite magmas can be direct mantle melts of peridotite in spite of experimental studies suggesting that mantle melts are invariably more mafic than basaltic andesites (Wyllie, 1984). The alternative idea that such andesite magmas are derived by partial melting of the subducted slab, and simply entrain the peridotite xenoliths as they rise through the mantle wedge on the way to the surface will be addressed in a separate section below. As a preliminary step, we have conducted some melt calculations using mineral/andesite liquid partition coefficients from Fujimaki et al. (1984), McKenzie and O'Nions (1991), Beattie (1994), Dunn and Sen (1994) and Green et al. (2000) in order to evaluate these two possibilities. The main goal of the calculations is to assess whether any well-characterized fertile peridotite samples could generate magmas similar to the Mexican andesites upon undergoing a reasonable degree of partial melting, leaving residues similar in composition to the most depleted of the El Peñon peridotite xenoliths. The calculations have focused on REE because of their coherence as a group and their incompatibility during melting.

Given the uncertainties of the actual composition of the source rocks for the Mexican high-magnesian siliceous andesites, we have elected to limit the calculation to simple batch melting (Shaw, 1970). Other more complicated melt models might also produce meaningful results when the starting parameters are varied, but these have not been explored in great detail. Our objective is to demonstrate plausibility with trace element modeling – even with a single model – that high-magnesian siliceous andesites can be derived from partial melting of mantle wedge peridotite. As the degree of fractional crystallization of a lava has been shown to be linked to Mg# (Cox et al., 1979), then melting rate estimates should be limited to rocks with high Mg# (>63). The composition of the El Peñon lavas (please see Table 1 of Blatter and Carmichael, 2001) satisfies this requirement. The results of the calculations for 1, 3, 5 and 10% partial melting are summarized on the diagram in Fig. 6.

The top half of the diagram in Fig. 6 shows the REE distribution patterns (thin black lines) in magmas derived by different degrees of partial melting of a peridotite slightly enriched in LREE as depicted by the upper bold line in the lower half of the diagram. The bold black lines in the top half of the diagram (shaded area) give the compositional range for the sixteen host lava samples

analyzed. The calculated patterns represented by the thin black lines in the top half of Fig. 6 show that REE compositions similar to those of the high-magnesian siliceous Mexican andesites can be produced by 1–5% (and possibly even as high as 7%) partial melting of a fertile spinel lherzolite source rock with HREE ~2.4–2.5 × chondrite, and slight LREE enrichment, yielding La_N/Yb_N of 1.7–1.8 (cf. Roden et al., 1988; Qi et al., 1995) and a residuum of amphibole-bearing spinel lherzolite (37% olivine, 40% orthopyroxene, 17.5% clinopyroxene, 4% spinel, and 1.5% amphibole).

An important constraint on these calculations imposed by the flat HREE patterns of the El Peñon lavas is that the solid residuum has to be garnet-free. Otherwise, the HREE would be held in the residuum resulting in much lower concentrations of these elements in the melt than are observed for the El Peñon andesites. A similar effect would be imparted on the derivative melts if there was a high abundance of amphibole in the source-rock residuum. However, when the amount of residual amphibole present is low (~1.5%), the HREE concentrations in the melt are similar to those observed for the high-magnesian siliceous Mexican andesites. When the residuum is "dry" (*i.e.*, amphibole-free), the HREE concentrations of the melt (at 1–5% melting of the original fertile rock) are too high to be considered comparable with the observed concentrations for the Mexican host lavas. In other words, the source for melts compositionally similar to the studied andesites has to be "wet" for amphibole to remain in the residuum at moderate degrees of partial melting. Additionally, higher degrees of melting, on the order of 10% of the original rock, would yield REE abundances in the product melt that are much lower than those observed for the Mexican host lavas.

The most LREE-depleted El Peñon lherzolite xenoliths (X-4 and X-12) have been evaluated as potential candidates for the solid residuum left in the mantle after andesite liquid generation and extraction (Fig. 6). However, none of the calculated residua following 1–5% melting of fertile spinel lherzolite corresponds perfectly to the compositions of these El Peñon lherzolite xenoliths. Besides the calculated elemental concentrations for the residua being higher than those for the X-4 and X-12 whole-rock samples, the overall patterns are different. The complex REE topology of these xenoliths is most likely the result of a long history of both depletion and enrichment. Although, none of the El Peñon peridotite xenoliths we have studied can be considered a direct residuum of generation and extraction of high-Mg andesite melts, the REE pattern of the xenolith X-12 resembles the patterns for 5–10% melting of slightly enriched fertile peridotite. Inasmuch as magmatic events in the region were probably multiple, the El Peñon xenoliths may represent residua after some earlier magmatic episodes not directly related to generation of their host andesite magmas.

4.4. Major oxide perspective on andesite origin

Experimental work by Hirose and Kawamoto (1995), Hirose (1997) and Blatter and Carmichael (2001) has shown that under water-saturated conditions in the upper mantle (10 kbar and 1000°C), partial melting of a fertile spinel lherzolite can produce liquids with major oxide compositions similar to those of the Mexican high-magnesian siliceous andesites. We have used some major oxide data in calculations to demonstrate whether these results support the 1–5% melting of spinel lherzolite to produce the Mexican andesites inferred from the trace element data. We have conducted the calculations for 1, 3, 5 and 10% melting using the batch melting equation (Shaw, 1970). Because the El Peñon peridotite xenoliths are small, it has been possible to measure the bulk rock major oxide concentrations needed for the modeling on only one sample of 0.5 g pooled from three closely spaced and nearly identical separate xenoliths. In addition, we have used nine other natural spinel lherzolite compositions characterized previously by others as examples of potential source rocks: KH-77-12 (Roden et al., 1988) and KLB-1 (Hirose and Kawamoto, 1995) both from Kilbourne Hole, New Mexico, M-38 from SE China (Qi et al., 1995), and DGO-165A, SLP-402, SLP-405, BCN-200 and SIN-3 from Mexico (Luhr and Aranda-Gomez, 1997). The Kilbourne Hole and Mexico samples were hosted by Tertiary and Quaternary magmas associated with extension in the Basin and Range Province. Two hypothetical peridotite residua have been used in the calculations: (a) one roughly corresponding to depleted spinel lherzolite from various locations (Dawson, 1980) with 45% olivine, 35% orthopyroxene, 12% clinopyroxene, 5% spinel, and 2% amphibole, and (b) the residuum we used for the REE melt calculations in the section above with 37% olivine, 40% orthopyroxene, 17.5% clinopyroxene, 4% spinel, and 1.5% amphibole. Because partition coefficients for most major elements are pressure-dependant, we have used values from the melting experiments of Blatter and Carmichael (2001), performed at 0.5–3.0 kbar (1000 ± 50 °C), only after applying a correction. Experiments by Hirose (1997) demonstrated that andesite-like melts can be produced by melting the Kilbourne Hole spinel lherzolite sample KLB-1 at 10 kbar, and therefore, we have extrapolated Blatter and Carmichael's major element partition

coefficients to this pressure as a minimum condition. Dependence of D (*i.e.*, mineral/liquid partition coefficient) on pressure can be approximated by the logarithmic function: $y = a * \ln(x)^2 + b$, where y is D mineral/liquid, x is pressure, and a and b are constants unique to the element. The $r^2 = 0.5–0.9$ for different elements.

The results of the calculations are summarized in Supplementary file A, where for comparison we also include data from the melting experiments of Hirose and Kawamoto (Hirose and Kawamoto, 1995) at H_2O-undersaturated conditions, and Hirose (1997) at H_2O-saturated conditions. Four out of nine potential starting rock compositions (KLB-1, KH-77-12, M-38, and DGO-165A) yield calculated melt compositions similar to the Mexican high-magnesian, siliceous andesites in the melting range of 1–10% at high a_{H2O}, with 1 to 5% melting producing the best match. The remaining five peridotite samples, including the El Peñon peridotite xenolith, do not produce liquids compositionally similar to the studied high-Mg andesites. While the liquids generated possess Mg numbers similar to those of the Mexican andesites, the former has unrealistically high SiO_2, and relatively low Al_2O_3 and CaO (Supplementary file A). It is clear, therefore, that these four peridotite samples are much too depleted in basaltic components (Al_2O_3 and CaO) and do not represent the composition of the source materials. In particular, El Peñon peridotite analyzed is quite poor in Al_2O_3 (2.12%) and CaO (2.12%), and produces the most silicic compositions (up to 73.5% SiO_2 at 10% melting; Supplementary file A).The five peridotites that produce liquids similar to El Peñon high-Mg, siliceous andesites are distinctly undepleted and contain very high amounts of basaltic components (up to about 4% of both Al_2O_3 and CaO).

These observations are in agreement with the notion that high-Mg, siliceous andesites can be produced by the melting of H_2O-saturated spinel lherzolites containing reasonably high concentrations of the basaltic components. It is also quite clear that the El Peñon peridotites (as represented by the analyzed pooled sample) are not the direct source of the high-Mg, siliceous andesite magma that brought them to the surface. Although major oxide concentrations suggest that the xenoliths can be the residual compositions after extraction of such liquids from originally undepleted, water-saturated spinel lherzolites, REE abundances do not support such a straight-forward interpretation. Overall, however, the results from calculations based on major oxide data are in good agreement with those obtained using the REE abundances.

4.5. Evaluation of a slab melting origin for the host lavas

Although some magma characteristics in continental arcs attributed to slab components can just as easily be acquired from the crust during ascent, the Mexican peridotite xenolith-bearing, high-magnesian, siliceous andesites at El Peñon probably ascended too fast to be subjected to significant crustal contamination (Plank and Langmuir, 1998). Therefore, their elemental and isotopic characteristics must reflect the nature of only the components in the source region. We have argued in favor of deriving these Mexican andesites from melting of metasomatized spinel peridotite in the mantle wedge. Nevertheless, it is instructive to evaluate the possibility of a slab melting origin for these lavas.

The arc-front, high-MgO andesites near El Peñon have many of the characteristics of adakitic lavas, including high Sr concentrations (>400 ppm) and low Y concentrations (<19 ppm), which yield Sr/Y ratios that are considered by some to be the result of melting a hydrous basaltic source under conditions that permit plagioclase to break down and garnet or amphibole to be the stable phases instead (Kay, 1978; Defant and Drummond, 1990; Kepezhinskas et al., 1995; Kepezhinskas et al., 1996; Kepezhinskas et al., 1997). This dehydration melting reaction produces a high-SiO_2 (>56 wt.%) melt phase that is enriched in Sr, Al_2O_3 (>15 wt.%) and Na_2O (>3.5 wt.%). The heavy rare earth elements (HREEs), much like Y, are retained in the amphibolite or garnet eclogite residue. Adakitic melts with these compositional parameters have been produced experimentally (Rapp et al., 1999) and are numerous in the plutonic roots of Archean arcs, but are not abundant in modern and present-day arcs. This is thought to reflect warmer conditions of the young oceanic crust that was being subducted in the Archean.

Few present-day arcs are consuming young/warm enough oceanic crust to produce slab melts, though other geodynamic factors also come into play. Based on geodynamic models, flat slab-subduction similar to what is observed in central Mexico does generate slab-melting conditions under certain circumstances. Finite element modeling by Manea et al. (2005) indicates that if temperature-dependent viscosities are used to model the mantle wedge, the slab descending beneath central Mexico becomes warm enough to melt.

Under this slab-melting hypothesis, these adakitic melts would infiltrate the overlying peridotite mantle wedge and react to become high-MgO andesite. This high-MgO andesite could entrain fragments of the melt-reacted peridotite and transport these xenoliths to the

surface. Indeed, such a scenario has been invoked for the origins of lavas with adakitic signatures that occur in several arcs worldwide (Defant and Kepezhinskas, 2001). Many of these adakitic lavas occur along with Nb-enriched arc basalts (NEAB, (Defant and Kepezhinskas, 2001)) that contain peridotite xenoliths with veins and inclusions of adakitic melt.

The scenario at El Peñon is incongruous with this slab melting hypothesis in several ways, including: (1) The El Peñon peridotite xenoliths do not exhibit any correlation between La and Ta (figure not reproduced here), which would be expected if they had been metasomatized by a silicic melt inasmuch as both La and Ta are compatible in silicic melt, but only La is compatible in hydrous fluid (Defant and Kepezhinskas, 2001). (2) The El Peñon peridotite xenoliths do not occur in NEAB and do not contain veins or inclusions of adakitic melt. NEAB is not found at the arc front in association with the Quaternary El Peñon andesites. Quaternary NEAB is found only in the middle to back portion of the Mexican Volcanic Belt (MVB) in this region (Blatter and Carmichael, 2001; Blatter et al., 2007). (3) Several of the andesites from the El Peñon region have been shown experimentally (Blatter and Carmichael, 1998; Blatter and Carmichael, 2001) to be in equilibrium with mantle-composition olivine (Fo_{90}) and orthopyroxene (En_{89}) and are consistent with melting of a peridotite source that has been metasomatized by hydrous fluids. High Ni and Cr concentrations in many of the El Peñon lavas also support this assertion. (4) The El Peñon andesites lack many of the other indicators of slab-melt association including: high Al_2O_3 (>15 wt.%), and abundant plagioclase phenocrysts. In fact, the El Peñon lavas are distinctive for their low Al_2O_3 contents and lack of plagioclase phenocrysts (Blatter and Carmichael, 1998; Blatter and Carmichael, 2001). We reiterate that lack of correlation between La and Ta in the xenoliths requires metasomatism by a hydrous fluid. Additionally, the extremely hydrous nature of the El Peñon lavas (3.5 to 6.5 wt.% H_2O) and their equilibrium with mantle olivine and orthopyroxene (Blatter and Carmichael, 1998; Blatter and Carmichael, 2001) are more consistent with these lavas resulting from low-percentage partial melting of a hydrous fluid-metasomatized peridotite.

As demonstrated above, garnet is not a likely phase in the residuum of the Mexican andesite source region. Having amphibole in the residuum explains the observed elemental distributions for the El Peñon andesites more convincingly. This phase is strongly enriched in REE, and is often a significant repository for Th, U and Sr. It can also be moderately enriched in HFSE, particularly Y (Table 1). Experimental work conducted by Fujimaki et al. (1984) and Zack et al. (1997) showed that the partition coefficient for Y is higher in amphibole than it is in clinopyroxene. Although Y compatibility in amphibole does not rival compatibility in garnet, there is considerably more of this element in amphibole than there is in clinopyroxene. The presence of amphibole in the residuum nicely accounts for the retention of Y during partial melting, while at the same time Sr is surrendered to the melt, principally by clinopyroxene, but also to some extent by amphibole. The low concentrations of Y and high Sr/Y ratio of the El Peñon andesites, therefore, are best explained by the interplay between these two phases, not by partial melting of a garnet-bearing slab.

5. Summary

The hornblende-bearing ultramafic xenoliths and clinopyroxene megaxenocrysts from near El Peñon in the central Mexican Volcanic Belt (MVB) were brought to the surface by a Quaternary hornblende high-Mg siliceous andesite, a rock type usually considered to evolved to be a direct product of mantle melting. These xenoliths have a record of melt depletion followed by metasomatism that allowed significant grain-to-grain differences in LREE concentrations to be preserved. This observation rules out pervasive chromatographic effects on all grains in the El Peñon xenoliths, and instead favors fluid or magma transport through the upper mantle from which they were extracted to have been channelized.

Finally, our calculations demonstrate that high-magnesian siliceous andesites like those at El Peñon, Mexico, can be produced by 1–5% melting of hydrous spinel lherzolite slightly enriched in LREE and compositionally similar to the xenoliths described by Roden et al. (1988) for Kilbourne Hole, New Mexico, by Qi et al. (1995) for SE China, and by Luhr and Aranda-Gomez (1997) for Durango (Mexico). Possibly because of multiple episodes of melt extraction and metasomatism, it is not possible to link the El Peñon lherzolite xenoliths genetically either to the high-magnesian siliceous andesites that delivered them to the surface or to the compositions close to the expected residues following melt extraction. However, these xenoliths could represent residua after earlier episodes of melting. Lava sample Z-353 (Table 2; Fig. 6) does not fit easily in the melting scheme advocated here. Its exceedingly high concentrations in the LREE ($L_N/Yb_N = 20.1$) seem to require either extremely low degrees of melting of hydrous spinel lherzolite (<1%), or the presence in the melt source region of strongly LREE-enriched garnet-free

materials. In any event, highly-Mg siliceous andesite can be a direct product of mantle wedge melting within the spinel lherzolite stability field.

Acknowledgments

We are indebted to Ian Carmichael and Rick Carlson for discussion and criticism of an earlier version of this manuscript. We also acknowledge the constructive reviews of two anonymous reviewers. This work was supported by grants from the National Science Foundation to SBM. We dedicate this paper to the memory of James F. Luhr, whom we believe to have been the anonymous reviewer with the most insightful yet friendly criticism of the first version of this manuscript.

Appendix A. Supplementery data

Supplementary data associated with this article can be found, in the online version, at doi:10.1016/j.epsl.2007.05.013.

References

Aizawa, Y., Tatsumi, Y., Yamada, H., 1999. Element transport by dehydration of subducted sediments: implications for arc and ocean island magmatism. Isl. Arc 8, 38–46.

Beattie, P., 1994. Systematics and energetics of trace-element partitioning between olivine and silicate melts; implications for the nature of mineral/melt partitioning. Chem. Geol. 117, 57–71.

Blatter, D.L., Carmichael, I.S.E., 1998. Hornblende peridotite xenoliths from central Mexico reveal the highly oxidized nature of subarc upper mantle. Geology 26, 1035–1038.

Blatter, D.L., Carmichael, I.S.E., 2001. Hydrous phase equilibria of a Mexican high-silica andesite; a candidate for a mantle origin? Geochim. Cosmochim. Acta 65, 4043–4065.

Blatter, D.L., Carmichael, I.S.E., Deino, A.L., Renne, P.R., 2001. Neogene volcanism at the front of the central Mexican volcanic belt; basaltic andesites to dacites, with contemporaneous shoshonites and high-TiO_2 lava. Geol. Soc. Amer. Bull. 113, 1324–1342.

Blatter, D.L., Farmer, G.L., Carmichael, I.S.E., 2007. A N–S transect across the central Mexican Volcanic Belt at ~100°W: spatial distribution, petrologic, geochemical, and isotopic characteristics of Quaternary volcanism. J. Petrol. 48, 901–950.

Bodinier, J.L., Vasseur, G., Vernieres, J., Dupuy, C., Fabries, J., 1990. Mechanisms of mantle metasomatism: geochemical evidence from the Lherz orogenic peridotite. J. Petrol. 31, 597–628.

Brandon, A.D., Draper, D.S., 1996. Constraints on the origin of the oxidation state of mantle overlying subduction zones; an example from Simcoe, Washington, USA, Geochim. Cosmochim. Acta 60, 1739–1749.

Canil, D., Scarfe, C.M., 1989. Origin of phlogopite in mantle xenoliths from Kostal Lake, Wells Gray Park, British Columbia. J. Petrol. 30, 1159–1179.

Chazot, G., Menzies, M.A., Harte, B., 1996. Determination of partition coefficients between apatite, clinopyroxene, amphibole, and melt in natural spinel lherzolites from Yemen; implications for wet melting of the lithospheric mantle. Geochim. Cosmochim. Acta 60, 423–437.

Chesley, J., Ruiz, J., Righter, K., Ferrari, L., Gomez-Tuena, A., 2002. Source contamination versus assimilation; an example from the Trans-Mexican volcanic arc. Earth Planet. Sci. Lett. 195, 211–221.

Church, S.E., Tatsumoto, M., 1975. Lead isotope relations in oceanic ridge basalts from the Juan de Fuca-Gorda Ridge area, N.E. Pacific Ocean. Contrib. Mineral. Petrol. 53, 253–279.

Conrad, W.K., Kay, R.W., 1984. Ultramafic and mafic inclusions from Adak Island; crystallization history, and implications for the nature of primary magmas and crustal evolution in the Aleutian Arc. J. Petrol. 25, 88–125.

Cox, K.G., Bell, J.D., Pankhurst, R.J., 1979. The Interpretation of Igneous Rocks. George Allen & Unwin Ltd, London. 450 pp.

Dawson, J.B., 1980. Kimberlites and their Xenoliths. Springer-Verlag, Berlin. 252 pp.

Defant, M.J., Drummond, M.S., 1990. Derivation of some modern arc magmas by melting of young subducted lithosphere. Nature 347, 662–665.

Defant, M.J., Kepezhinskas, P., 2001. Evidence suggests slab melting in arc magmas. EOS 82, 65–69.

DeMets, C., Gordon, R.G., Argus, D.F., Stein, S., 1990. Current plate motions. Geophys. J. Int. 101, 425–478.

Dickinson, W.R., Lawton, T.F., 2001. Carboniferous to Cretaceous assembly and fragmentation of Mexico. Geol. Soc. Amer. Bull. 113, 1142–1160.

Dunn, T., Sen, C., 1994. Mineral/matrix partition coefficients for orthopyroxene, plagioclase, and olivine in basaltic to andesitic systems; a combined analytical and experimental study. Geochim. Cosmochim. Acta 58, 717–733.

Fujimaki, H., Tatsumoto, M., Aoki, K.-i., 1984. Partition coefficients of Hf, Zr, and REE between phenocrysts and groundmasses. J. Geophys. Res., B 89, 662–672 (Suppl.).

Galer, J.G., O'Nions, R.K., 1989. Chemical and isotopic studies of ultramafic inclusions from the San Carlos Volcanic Field, Arizona: a bearing on their petrogenesis. J. Petrol. 30, 1033–1064.

Green, T.H., Blundy, J.D., Adam, J., Yaxley, G.M., 2000. SIMS determination of trace element partition coefficients between garnet, clinopyroxene and hydrous basaltic liquids at 2–7.5 GPa and 1080–1200 degrees C. Lithos 53, 165–187.

Hart, S.R., 1984. A large scale isotope anomaly in the Southern Hemisphere mantle. Nature 309, 753–757.

Hasenaka, T., Carmichael, I.S.E., 1985. The cinder cones of Michoacan–Guanajuato, central Mexico; their age, volume and distribution, and magma discharge rate. J. Volcanol. Geotherm. Res. 25, 105–124.

Hirose, K., 1997. Melting experiments on lherzolite KLB-1 under hydrous conditions and generation of high-magnesian andesitic melts. Geology 25, 42–44.

Hirose, K., Kawamoto, T., 1995. Hydrous partial melting of lherzolite at 1 GPa; the effect of H_2O on the genesis of basaltic magmas. Earth Planet. Sci. Lett. 133, 463–473.

Hofmann, A.W., 1997. Mantle geochemistry; the message from oceanic volcanism. Nature 385, 219–229.

Iwamori, H., 2000. Deep subduction of H_2O and deflection of volcanic chain towards backarc near triple junction due to lower temperature. Earth Planet. Sci. Lett. 181, 41–46.

Karig, D.E., Cardwell, R.K., Moore, G.F., Moore, D.G., 1978. Late Cenozoic subduction and continental margin truncation along the northern Middle America Trench. GSA Bull. 89, 265–276.

Kay, R.W., 1978. Aleutian magnesian andesites; melts from subducted Pacific Ocean crust. J. Volcanol. Therm. Res. 117–132.

Kelemen, P.B., Dick, H.J.B., Quick, J.E., 1992. Formation of harzburgite by pervasive melt/rock reaction in the upper mantle. Nature 358, 635–641.

Kepezhinskas, P.K., Defant, M.J., Drummond, M.S., 1995. Na metasomatism in the island-arc mantle by slab melt-peridotite interaction; evidence from mantle xenoliths in the North Kamchatka Arc. J. Petrol. 36, 1505–1527.

Kepezhinskas, P., Defant, M.J., Drummond, M.S., 1996. Progressive enrichment of island arc mantle by melt–peridotite interaction inferred from Kamchatka xenoliths. Geochim. Cosmochim. Acta 60, 1217–1229.

Kepezhinskas, P.K., McDermott, F., Defant, M.J., Hochstaedter, A.G., Drummond, M.S., Hawkesworth, C.J., Koloskov, A.V., Maury, R.C., Bellon, H., 1997. Trace element and Sr–Nd–Pb isotopic constraints on a three-component model of Kamchatka Arc petrogenesis. Geochim. Cosmochim. Acta 61, 577–600.

Kerrick, D.M., Connolly, J.A.D., 2001a. Metamorphic devolatilization of subducted oceanic metabasalts; implications for seismicity, arc magmatism and volatile recycling. Earth Planet. Sci. Lett. 189, 19–29.

Kerrick, D.M., Connolly, J.A.D., 2001b. Metamorphic devolatilization of subducted marine sediments and the transport of volatiles into the Earth's mantle. Nature 411, 293–296.

Klein, E.M., Langmuir, C.H., 1987. Golbal correlations of ocean ridge basalt chemistry with axial depth and crustal thickness. J. Geophys. Res. 92, 8089–8115.

Luhr, J.F., Aranda-Gomez, J.J., 1997. Mexican peridotite xenoliths and tectonic terranes; correlations among vent location, texture, temperature, pressure, and oxygen fugacity. J. Petrol. 38, 1075–1112.

Manea, V.C., Kostoglodov, V., Sewell, G., 2005. Thermo-mechanical model of the mantle wedge in central Mexican subduction zone and a blob tracing approach for the magma transport: Physics Earth Planet. Interiors 149, 165–186.

Maury, R.C., Defant, M.J., Joron, J.-L., 1992. Metasomatism of the sub-arc mantle inferred from trace elements in Philippine xenoliths. Nature 360, 661–663.

McDonough, W.F., Sun, S.S., 1995. The composition of the Earth. Chem. Geol. 120, 223–253.

McInnes, B.I.A., Cameron, E.M., 1994. Carbonated, alkaline hybridizing melts from a sub-arc environment; mantle wedge samples from the Tabar-Lihir-Tanga-Feni Arc, Papua New Guinea. Earth Planet. Sci. Lett. 122, 125–141.

McInnes, B.I.A., Gregoire, M., Binns, R.A., Herzig, P.M., Hannington, M.D., 2001. Hydrous metasomatism of oceanic sub-arc mantle, Lihir, Papua New Guinea; petrology and geochemistry of fluid-metasomatised mantle wedge xenoliths. Earth Planet. Sci. Lett. 188, 169–183.

McKenzie, D., O'Nions, R.K., 1991. Partial melt distributions from inversion of rare earth element concentrations. J. Petrol. 32, 1021–1091.

Mukasa, S.B., Shervais, J.W., 1999. Growth of subcontinental lithosphere; evidence from repeated dike injections in the Balmuccia lherzolite massif, Italian Alps. In: van der Hilst, R.D., McDonough, W.F. (Eds.), Composition, deep structure and evolution of continents, vol. 48. Elsevier, Amsterdam, pp. 287–316.

Mukasa, S.B., McCabe, R., Gill, J.B., 1987. Pb-isotopic compositions of volcanic rocks in the West and East Philippine island arcs: presence of the Dupal isotopic anomaly. Earth Planet. Sci. Lett. 84, 153–164.

Mukasa, S.B., Shervais, J.W., Wilshire, H.G., Nielson, J.E., 1991. Intrinsic Nd, Pb, and Sr isotopic heterogeneities exhibited by the Lherz alpine peridotite massif, French Pyrenees. J. Petrol. 117–134.

Navon, O., Stolper, E., 1987. Geochemical consequences of melt percolation: the upper mantle as a chromatographic column. J. Geol. 95, 285–307.

Nimz, G.J., Cameron, K.L., Niemeyer, S., 1993. The La Olivina pyroxenite suite and the isotopic compositions of mantle basalts parental to the mid-Cenozoic arc volcanism of northern Mexico. J. Geophys. Res. 98, 6489–6509.

Nimz, G.J., Cameron, K.L., Niemeyer, S., 1995. Formation of mantle lithosphere beneath northern Mexico; chemical and Sr–Nd–Pb isotopic systematics of peridotite xenoliths from La Olivina. J. Geophys. Res., B, [Solid Earth Planets] 100, 4181–4196.

Pardo, M., Suarez, G., 1995. Shape of the subducted Rivera and Cocos plates in southern Mexico; seismic and tectonic implications. J. Geophys. Res., B, [Solid Earth and Planets] 100, 12,357–312,373.

Parkinson, I.J., Arculus, R.J., 1999. The redox state of subduction zones; insights from arc-peridotites. Chem. Geol. 160, 409–423.

Pasquarè, G., Ferrari, L., Garduno, V.H., Tibaldi, A., Vezzoll, L., 1991. Geologic map of the central sector of the Mexican volcanic belt, states of Guanajuato and Michoacan, Mexico, Map and Chart Series (Geological Society of America), MCH072. 1 pp.

Peacock, D.C.P., 2001. The temporal relationship between joints and faults. J. Struct. Geol. 23, 329–341.

Petrone, C.M., Francalanci, L., Carlson, R.W., Ferrari, L., Conticelli, S., 2003. Unusual coexistence of subduction-related and intraplate-type magmatism; Sr, Nd and Pb isotope and trace element data from the magmatism of the San Pedro-Ceboruco Graben (Nayarit, Mexico). Chem. Geol. 193, 1–24.

Plank, T., Langmuir, C.H., 1998. The chemical composition of subducting sediment and its consequences for the crust and mantle. Chem. Geol. 145, 325–394.

Qi, Q., Taylor, L.A., Zhou, X., 1995. Petrology and geochemistry of mantle peridotite xenoliths from SE China. J. Petrol. 36, 55–79.

Rapp, R.P., Shimizu, N., Norman, M.D., Applegate, G.S., 1999. Reaction between slab-derived melts and peridotite in the mantle wedge; experimental constraints at 3.8 GPa. Chem. Geol. 160, 335–356.

Righter, K., 2000. A comparison of basaltic volcanism in the Cascades and western Mexico; compositional diversity in continental arcs. Tectonophysics 318, 99–117.

Roden, M.F., Irving, A.J., Murthy, V.R., 1988. Isotopic and trace element composition of the upper mantle beneath a young continental rift: results from Kilbourne Hole, New Mexico. Geochim. Cosmochim. Acta 52, 461–473.

Scarfe, C.M., Brearley, M., 1987. Mantle xenoliths; melting and dissolution studies under volatile-free conditions. In: Nixon, P.H. (Ed.), Mantle Xenoliths. John Wiley and Sons, pp. 599–608.

Sen, G., Frey, F.A., Shimizu, N., Leeman, W.P., 1993. Evolution of the lithosphere beneath Oahu, Hawaii: rare earth element abundances in mantle xenoliths. Earth Planet. Sci. Lett. 119, 53–69.

Shaw, D.M., 1970. Trace element fractionation during anatexis. Geochim. Cosmochim. Acta 34, 237–243.

Shimizu, N., Le Roex, A.P., 1986. The chemical zoning of augite phenocrysts in alkaline basalts from Gough Island, South Atlantic. J. Volcanol. Geotherm. Res. 29, 159–188.

Shimizu, N., Semet, M.P., Allègre, C.J., 1978. Geochemical applications of quantitative ion-microprobe analysis. Geochim. Cosmochim. Acta 42, 1321–1334.

Smith, A.D., 1999. The Nd–Sr–Pb isotopic record in abyssal tholeiites from the Gulf of California region, western Mexico; no evidence for a gulf mouth plume. Int. Geol. Rev. 41, 921–931.

Sun, S.S., McDonough, W.F., 1989. Chemical and isotopic systematics of oceanic basalts; implications for mantle composition and processes. Geol. Soc. Spec. Pub. 42, 313–345.

Takahashi, E., 1980. Thermal history of lherzolite xenoliths; I, Petrology of lherzolite xenoliths from the Ichinomegata Crater, Oga Peninsula, Northeast Japan. Geochim. Cosmochim. Acta 44, 1643–1658.

Tanaka, T., Aoki, K.-i., 1981. Petrogenic implications of REE and Ba data on mafic and ultramafic inclusions from Itinome-gata, Japan. J. Geol. 89, 369–390.

Ulmer, P., Trommsdorff, V., 1995. Serpentine stability to mantle depths and subduction-related magmatism. Science 268, 858–861.

Verma, S.P., 1999. Geochemistry of evolved magmas and their relationship to subduction-unrelated mafic volcanism at the volcanic front of the central Mexican volcanic belt. J. Volcanol. Geotherm. Res. 93, 151–171.

Verma, S.P., Nelson, S.A., 1989. Isotopic and trace element constraints on the origin and evolution of alkaline and calc–alkaline magmas in the northwestern Mexican volcanic belt. J. Geophys. Res., B, [Solid Earth and Planets] 94, 4531–4544.

Vidal, P., Dupuy, C., Maury, R.C., Richard, M., 1989. Mantle metasomatism above subduction zones; trace-element and radiogenic isotope characteristics of peridotite xenoliths from Batan Island (Philippines). Geology 17, 1115–1118.

Wallace, P.J., Carmichael, I.S.E., 1994. Petrology of Volcan Tequila, Jalisco, Mexico; disequilibrium phenocryst assemblages and evolution of the subvolcanic magma system. Contrib. Mineral. Petrol. 117, 345–361.

Wilshire, H.G., Meyer, C.E., Nakata, J.K., Calk, L.C., Shervais, J.W., Nielson, J.E., Schwarzman, E.C., 1988. Mafic and Ultramafic Xenoliths from Volcanic Rocks of the Western United States. U. S. Geol. Survey Prof. Pap. 1443, USGS, p. 179.

Wilson, M., 1989. Igneous Petrogenesis. Unwin Hyman, London. 466 pp.

Wood, B.J., Virgo, D., 1989. Upper mantle oxidation state; ferric iron contents of lherzolite spinels by ^{57}Fe Moessbauer spectroscopy and resultant oxidation fugacities. Geochim. Cosmochim. Acta 53, 1277–1291.

Wyllie, P.J., 1984. Constraints imposed by experimental petrology on possible and impossible magma sources and products. Philos. Trans. R. Soc. Lond. Ser. A: Math. Phys. Sci. 310, 439–456.

Zack, T., Foley, S.F., Jenner, G.A., 1997. A consistent partition coefficient set for clinopyroxene, amphibole and garnet from laser ablation microprobe analysis of garnet pyroxenites from Kakanui, New Zealand, Neues Jahrbuch fuer Mineralogie. Abhandlungen 172, 23–41.